Biomaterials Science

Engineering release kinetics with polyelectrolyte multilayers to modulate TLR signalling and promote immune tolerance

Journal:	*Biomaterials Science*
Manuscript ID	BM-ART-12-2018-001572.R1
Article Type:	Paper
Date Submitted by the Author:	21-Dec-2018
Complete List of Authors:	Tostanoski, Lisa; University of Maryland at College Park, Fischell Department of Bioengineering Eppler, Haleigh; University of Maryland at College Park, Fischell Department of Bioengineering Xia, Boyan; University of Maryland at College Park, Fischell Department of Bioengineering Zeng, Xiangbin; University of Maryland at College Park, Fischell Department of Bioengineering Jewell, Christopher; University of Maryland at College Park, Fischell Department of Bioengineering

Biomaterials Science

ARTICLE

Engineering release kinetics with polyelectrolyte multilayers to modulate TLR signalling and promote immune tolerance

Received 00th January 20xx,
Accepted 00th January 20xx

DOI: 10.1039/x0xx00000x

www.rsc.org/

Lisa H. Tostanoski,[‡,a] Haleigh B. Eppler,[‡,a,b] Boyan Xia,[a] Xiangbin Zeng,[a] and Christopher M. Jewell [a,b,c,d,e,f*]

Autoimmune disorders, such as multiple sclerosis and type 1 diabetes, occur when immune cells fail to recognize "self" molecules. Recently, studies have revealed aberrant inflammatory signaling through pathogen sensing pathways, such as toll-like receptors (TLRs), during autoimmune disease. Therapeutic inhibition of these pathways might attenuate disease development, skewing disease-causing inflammatory cells towards cell types that promote tolerance. Delivering antagonistic ligands to a TLR upstream of an inflammatory signaling cascade, TLR9, has demonstrated exciting potential in a mouse model of MS; however, strategies that enable sustained delivery could reduce the need for repeated administration or enhance therapeutic efficacy. We hypothesized that GpG, an oligonucleotide TLR9 antagonist – which is inherently anionic, could be self-assembled into polyelectrolyte multilayers (PEMs) with a cationic, degradable poly(β-amino ester) (Poly1). We hypothesized that degradable Poly1/GpG PEMs could promote sustained release of GpG and modulate inflammatory immune cell functions. Here we demonstrate layer-by-layer assembly of degradable PEMs, as well as subsequent degradation and release of GpG. Following assembly and release, GpG maintains the ability to reduce dendritic cell activation and inflammatory cytokine secretion, restrain TLR9 signaling, and polarize myelin specific T cells towards regulatory phenotypes and functions in primarily immune cells. These results indicate that degradable PEMs may be able to promote tolerogenic immune function in the context of autoimmunity.

Introduction

Autoimmune diseases are marked by misidentification and attack of "self" tissues – such as myelin, which is attacked in multiple sclerosis (MS) – by cells of the adaptive immune system (i.e., B and T cells). However, recent research has revealed increased stimulation of innate inflammatory pathways, such as toll like receptor (TLR) signaling, during mouse models and human autoimmune disease.[1-8] For example, signaling through TLR9, a pattern recognition receptor typically responsible for sensing DNA structures common in bacteria, is upregulated in human autoimmune disease and a mouse model of MS, experimental autoimmune encephalomyelitis (EAE). Induction of EAE in TLR9 knockout mice attenuates disease compared with wild-type mice, suggesting an important role for TLR9 in disease development and progression.[8] Further, administration of GpG – an antagonistic regulatory ligand of TLR9 that down-regulates inflammatory signaling – drives partial control of a relapsing-remitting form of EAE.[9, 10] Together, these findings support new opportunities to target the TLR9 pathway to control inflammation and promote immune tolerance.

The kinetics of autoimmune disease development and maintenance – and the underlying inflammation – span weeks to decades.[8] As a result, an important clinical consideration is the dosing schedule. Clinically-approved therapies for MS designed to deliver anti-inflammatory or regulatory immune signals are plagued by a need for regular, life-long dosing.[11] This challenge has motivated the exploration of novel strategies that maintain efficacy while providing more targeted delivery, continuous release, or both. As one example, a first-line treatment for MS – glatiramer acetate – was recently approved for some patients as a 3x weekly injection.[12, 13] This improvement over the traditional daily injection provides increased compliance and convenience, particularly for a

[a.] Fischell Department of Bioengineering, A. James Clark Hall, Room 5110, 8278 Paint Branch Drive, College Park, Maryland 20742, USA.
[b.] Molecular and Cellular Biology, Biological Science Training Program, Biological Science Training Program, Biology-Psychology Building, Room 1247, 4094 Campus Drive, College Park, Maryland 20742, USA.
[c.] Department of Microbiology and Immunology, University of Maryland School of Medicine, 685 West Baltimore Street, HSF-I Suite 380, Baltimore, Maryland 21201, USA.
[d.] Marlene and Stewart Greenebaum Cancer Center, Executive Office, Suite N9E17, 22 S. Greene Street, Baltimore, Maryland 21201, USA.
[e.] United States Department of Veterans Affairs, VA Maryland Health Care System, 10 North Greene Street, Baltimore, Maryland 21201, USA
[f.] Robert E. Fischell Institute for Biomedical Devices, A. James Clark Hall, Room 5102, 8278 Paint Branch Drive, College Park, Maryland 20742, USA.
‡ These authors equally contributed to this manuscript.
* To whom correspondence should be addressed (E-mail: cmjewell@umd.edu).

Electronic Supplementary Information (ESI) available: [details of any supplementary information available should be included here]. See DOI: 10.1039/x0xx00000x

disease such as MS where patients suffer from decreasing motor control.

In light of the challenges discussed above, biomaterials offer unique features to tackle autoimmune disease, including co-delivery of multiple signals, protection of biologic cargo, and controlled release.[14, 15] We recently exploited electrostatics to design biomaterial strategies to co-deliver GpG with a myelin peptide implicated in EAE, myelin oligodendrocyte glycoprotein (MOG)[16, 17]. In one approach, these signals were self-assembled into polyelectrolyte multilayers (PEMs), nano-scale coatings formed in a layer-by-layer fashion through electrostatics and other non-covalent interactions.[15, 18-20] Uniquely, these structures – which we termed immune PEMs (iPEMs) – were composed entirely of immune signals and enabled attenuation of EAE. Because of their modularity, PEMs also provide an opportunity to investigate the impact of controlling the kinetics with which GpG or other regulatory signals are delivered to immune cells, as well as the resulting impact on inflammation. To investigate this idea, we designed PEMs from GpG and a poly(β-amino ester) (Poly1), a cationic, degradable polymer widely exploited in nucleic acid delivery.[21, 22] In this scheme, we used Poly1 to enable controlled release and as a structural component to support electrostatic interaction with GpG oligonucleotide.

We hypothesized juxtaposition of Poly1 and GpG would create degradable PEMs that allow rational assembly, followed by slow release of cargo to restrain inflammation and bias immune cells toward regulatory populations that promote tolerance. Here we first demonstrate layer number-dependent incorporation of GpG in PEMs across size scales and geometries. Upon incubation in physiologically-relevant conditions, these assemblies break down, releasing GpG from coated substrates over time. The released GpG maintains biologic function, restraining primary dendritic cell (DC) activation and inflammatory cytokine secretion. Further, the molecular specificity of GpG interaction with the TLR9 receptor and the related signal transduction is unchanged by assembly and release from these degradable PEMs. Lastly, GpG released from the PEMs polarizes myelin-specific T cells away from inflammatory functions and towards a phenotype demonstrated to promote tolerance, regulatory T cells (T_{REGS}). Together, these results support modification of iPEMs with degradable components as platform to modulate inflammatory TLR signaling associated with autoimmune disease.

Materials and Methods

Reagents

MOG peptide (MOG_{35-55}, MEVGWYRSPFSRVVHLYRNGK), was purchased from Genscript with HPLC purification to > 98% purity. Oligonucleotides, including TLR9 agonist CpG (5-T*C*C*A*T*G*A*C*G*T*T*C*C*T*G*A*C*G*T*T-3), TLR9 antagonist GpG (5-T*G*A*C*T*G*T*G*A*A*G*G*T*T*A*G*A*G*A*T*G*A-3), and irrelevant control nucleotide (CTRL, 5-T*C*C*T*G*A*G*C*T*T*G*A*A*G*T-3), modified with phosphorothioate backbones, were purchased from IDT.

Poly(β-amino ester) (Poly1) synthesis

A Michael-type addition reaction was used to synthesize Poly1, as described previously[21]. In brief, 9 mmol of 4,4'-trimetylenepiperidine was dissolved in anhydrous THF to form a 500 mg/mL solution. The solution was added to 9 mmol of 1,4-butanediol diacrylate, then heated to 50°C with stirring for 16 h. After cooling to room temperature, ice-cold diethyl ether was used to precipitate out the resultant polymer under vigorous stirring. Poly1 was then collected, washed with additional diethyl ether, and lyophilized. Before use in experiments, Poly1 was characterized by gel permeation chromatography and H-NMR, as previously described.[23]

Preparation and coating of planar substrates

A diamond-tipped saw (Micro Automation) was used to cut quartz slides (VWR) and silicon wafers (Silicon Inc.) into 5 mm x 25 mm chips for studies on planar substrates. Sequential rinsing in acetone, ethanol, methanol, and water was used to clean substrate surfaces. Following the rinse in water, substrates were dried under a stream of air and treated with an oxygen plasma system (Branson Barrel Resist Stripper). Base layers were next deposited on prepared substrates as previously reported [16, 24, 25]. Briefly, chips were incubated in 20 mM poly(ethyleneimine) (PEI, Polysciences, Inc.) with 50 mM NaCl and 5 mM HCl for 5 min, followed by two washes in water for 1 min each. Chips were then incubated in 20 mM poly(sodium 4-styrene sulfonate) (SPS, Sigma-Aldrich) with 50 mM NaCl for 5 min, and washed two more times with water. This cycle was repeated for a total of ten bilayers to generate $(PEI/SPS)_{10}$ substrates using a DR3 dipping robot (Riegler & Kirstein GmbH) similar to previous reports.[25] Following the tenth dipping cycle, coated chips were dried under air and stored at room temperature until subsequent coating with degradable PEMs.

Degradable PEM deposition

Poly1 was dissolved at 0.55 mg/mL in 1X PBS (Corning) and GpG was dissolved at 2mg/mL in water. Degradable PEMs were assembled by incubating base layer-coated substrates in Poly1 for 5 min, washing twice in water for 1 min, incubating in GpG for 5 min, and washing two additional times in water. To deposit the desired number of Poly1/GpG bilayers, this cycle was repeated. In some studies, GpG cargo was replaced with CTRL to allow for the synthesis of control PEMs to isolate GpG-specific effects on cells.

Degradable PEM fluorescence image analysis

To characterize cargo incorporation, degradable PEMs were synthesized using GpG labeled with a fluorescent tag (Cy5, Mirus). For planar substrates, quartz chips were coated with base layers followed by one, two, or three cycles of Poly1/Cy5-GpG, as described above. In colloidal substrate experiments, 5

μm polystyrene beads (Polysciences) were coated with one, two, or three bilayers of Poly1/Cy5-GpG as above, with the addition of centrifugation steps between incubations to collect particles. For each substrate, fixed exposure time fluorescence microscopy was used to visualize signal intensity as a function of the number of bilayers deposited. Further, pixel intensity analysis was performed using ImageJ software to quantify signal after each bilayer deposition.

Quantitative degradable PEM growth characterization

In some experiments, Poly1/GpG PEMs were deposited on silicon chips. Every two or eight bilayers, chips were dried under air and measured using a Stokes Ellipsometer (Gaertner Scientific) to quantify film thickness. At each measurement step, average thickness was calculated by measuring three locations on at least three separate substrates. In studies designed to measure relative cargo loading, degradable PEMs were assembled on quartz chips and UV-Visible spectrophotometry was used to record the absorbance values at 260 nm every two or eight bilayers. In some studies, scans from 240 nm to 320 nm were performed to monitor for a peak of signal at 260 nm, characteristic of nucleic acids. As above, measurements were recorded at three locations on independently-prepared substrates and averaged. Relative GpG loading was indicated by the absorbance value at 260 nm.

Kinetic release studies

$(Poly1/GpG)_{100}$ PEMs were incubated in 1 mL of 1X PBS (Corning) at 37°C with shaking. At indicated time points, quartz and silicon substrates were removed and dried under air. Time elapsed during measurement was not included in quantification of release time. Coated quartz substrates and release solutions were measured using UV-Visible spectrophotometry to record absorbance values from 190 nm to 500 nm. For quartz chips, measurements were recorded at three locations on at least three independent substrates and relative GpG loading was indicated by the absorbance at 260 nm. For release solutions, absorbance values of three independently-prepared solutions were recorded with mixing between each measurement. GpG loading was quantified by converting the absorbance at 260 nm to concentration and mass released using a known standard.

Cells and animals

All studies involving mice (as a source of primary cells) were carried out in compliance with federal, state, and local laws and followed institutional guidelines, including the Guide for the Care and Use of Laboratory Animals and the Animal Welfare Act. All experiments were reviewed and approved by the University of Maryland's Institutional Animal Care and Use Committee (IACUC).

Dendritic cell activation

A $CD11c^+$ magnetic kit (Miltenyi Biotec) was used to isolate DCs from the spleens of naïve C57BL/6J mice (The Jackson Laboratory) according to the manufacturer's instructions. Cells were plated at 1 x 10^5 cells/well in RPMI 1640 media (Lonza), supplemented with 10% fetal bovine serum (Corning), 2 mM L-glutamine (Gibco), 55 μM β-mercaptoethanol (Sigma-Aldrich), 1 X Non-Essential Amino Acids (Fisher Scientific), 10mM HEPES (Fisher Scientific), and 1 X Pen/Strep (Gibco). For activation studies, cells, with the exception of media only controls, were activated with soluble CpG (1 μg/well). Soluble GpG (10 μg) and CTRL (10 μg) were added to CpG-treated wells for controls. Release solutions from incubation of $(Poly1/GpG)_{100}$ or $(Poly1/CTRL)_{100}$ PEMs for indicated time points, as described above, were added to additional CpG-treated wells. Matched doses of soluble GpG and CTRL, corresponding to each release time point (i.e., days 1, 3, 5, 7), were also incubated with CpG-treated wells. After 16 h of incubation, cells were collected, washed twice in 1 X PBS with 1% BSA (FACS buffer), and blocked with anti-CD16/CD32 (BD Biosciences). Cells were then incubated with anti-CD40, anti-CD80, and anti-CD86 (BD Biosciences) for 20 min at room temperature. After incubation, cells were washed two more times as above, and resuspended in DAPI for analysis by flow cytometry. FlowJo software (Tree Star) was used to conduct all data analysis.

TLR9 signalling assay

HEK-Blue mTLR9 reporter cells were plated at 5 x 10^5 cells/well in HEK-Blue Detection Media per the manufacturer's instructions (InvivoGen). Control samples included media only, a vehicle control (PBS), and cells treated with a TLR4 agonist, lipopolysaccharide (LPS, 0.2 μg/well, InvivoGen) to verify TLR9-specific reporter signal. All remaining wells were treated with 1 μg/well of soluble CpG. $(Poly1/GpG)_{100}$ and $(Poly1/CTRL)_{100}$ PEMs were incubated in 1 mL of 1 X PBS at 37°C with agitation for the indicated amount of time, as described above, and release solutions were added to CpG-treated wells. Matched doses of soluble GpG and soluble CTRL were also prepared and added to CpG-treated wells. Cultures were incubated for 18 hours and TLR9 signalling was quantified measuring the absorbance at 620 nm. Relative TLR9 signalling was determined by normalizing absorbance values to the average absorbance of control wells treated with media only.

Transgenic T cell proliferation

To test how degradable PEMs impact antigen-specific T cell expansion, DCs from C57BL/6J mice were isolated, as above. Control wells of cells treated with: i) media only, ii) soluble MOG peptide alone (0.2 μg/well), iii) soluble CpG alone (1μg/well), and iv) soluble MOG (0.2 μg/well) + soluble CpG (1 μg/well) were prepared. All other wells were treated with soluble MOG (0.2 μg/well) and CpG (1μg/well) and the following treatment groups were tested: i) soluble GpG (10 μg/well), ii) soluble CTRL (10 μg/well), iii) release solutions from either $(Poly1/GpG)_{100}$ or $(Poly1/CTRL)_{100}$ PEMs, as described above, and iv) soluble GpG or CTRL at a matched dose for the release solution at each time point, as above. 16h later, $CD4^+$ T cells were isolated from the spleens of 2D2 mice (C57BL/6-Tg(Tcra2D2,Tcrb2D2)1Kuch/J, The Jackson

Laboratory), which have T cell receptors specific to MOG. These cells were collected using a magnetic isolation kit (StemCell Technologies), according to the manufacturer's instructions, and then incubated with a cell proliferation dye (CFSE, eBioscience). Labeled cells were then washed, and 2.5 x 10^5 labelled cells were added to each well of the DC cultures. After 72 h of co-culture, cells were collected, washed and blocked, as above. Blocked cells were then incubated with anti-CD4 (BD Biosciences) for 20 min at room temperature, washed, and resuspended in DAPI for analysis by flow cytometry.

Transgenic T cell phenotype

In some studies, DC cultures were prepared, as above, and $CD4^+$ T cells isolated from the spleens of 2D2 mice were added to cultures without incubation with the cell proliferation dye. After 72 h of co-culture, these cells were analysed for markers of T cell phenotype. First, cells were collected, washed, and stained with antibodies against surface markers CD4 and CD25. Cells were then washed to remove unbound antibody and fixed and permeabilized using a Foxp3/Transcription Factor staining buffer set according to the manufacturer's instructions (eBiosceince). Cells were then stained with anti-Fopx3, washed twice, and resuspended in FACS buffer for flow cytometry analysis.

ELISA

Supernatants from DC activation cultures or DC-2D2 T cell co-cultures, described above, were collected analyzed by ELISA according to manufacturer's instructions for the secretion of IL-6 (BD Biosciences).

Results

Degradable PEMs exhibit layer-dependent incorporation of cargo

To ascertain the ability of Poly1 and GpG to co-assemble using a layer-by-layer approach, we first attempted to build degradable PEMs on planar substrates using fluorescently-labeled GpG. Fixed exposure fluorescence microscopy revealed a qualitative increase in image brightness with increasing number of bilayers (Fig. 1A). This observation was confirmed through quantitative pixel intensity analysis of images after one, two, and three cycles of Poly1/GpG deposition (Fig. 1B). Analogous results were observed when polystyrene microparticles were coated with Poly1/GpG (Fig. 1C-1D), supporting the potential of the approach for colloidal substrates useful in many cell and animal therapeutic delivery schemes.

To quantify thes assembly process, Poly1/GpG PEMs were assembled on planar substrates of either silicon or quartz. During deposition of 8 bilayers (16 layers), a linear increase in film thickness (R^2=0.982) was measured by ellipsometry, with $(Poly1/GpG)_8$ films exhibiting a final thickness of ~110 nm (Fig. 2A). Linear growth (R^2=0.991) was also observed when 56 bilayers were deposited, yielding a final thickness of ~320nm (Fig. 2B). To verify the increase in thickness was due to layer-dependent incorporation of cargo, spectrophotometric analysis was performed on coated quartz substrates. Consistent with the thickness data, a linear increase in relative GpG loading was observed through eight (R^2=0.992) or 56 (R^2=0.991) bilayers (Fig. 2C-2D). Further, spectrum scans confirmed a peak in signal at 260 nm, characteristic of nucleic acids, supporting an increase is absorbance due to incorporation of GpG (Fig. 2E). Together the results of Fig.s 1 and 2 demonstrate the potential to control GpG incorporation into Poly1/GpG PEMs in a precise fashion by varying the number of bilayers deposited.

Poly1/GpG PEMs enable controlled release of cargo

The backbone of Poly1 contains hydrolysable ester bonds.[21, 22] Thus, we hypothesized Poly1/GpG PEMs would degrade over time. To measure the kinetics of degradation and corresponding release of cargo, release studies were conducted by incubating $(Poly1/GpG)_{100}$ PEMs on silicon or quartz substrates in PBS. Spectrophotometric analysis revealed a time-dependent increase in mass of nucleic acid cargo released from silicon substrates. (Fig. 3A). Over three days of incubation, ~50μg of GpG was released per cm^2, resulting in ~100 μg of total mass released into solution. Similarly, incubation of quartz substrates coated with $(Poly1/GpG)_{100}$ revealed a decrease in absorbance signal at the characteristic wavelength of GpG (Fig. 3B), while a time-dependent increase in GpG mass was detected in the release solutions from these substrates (Fig. 3C). These results indicate release of GpG into solution corresponds to decreased signal from the $(Poly1/GpG)_{100}$ assembly, supporting the hypothesis of controlled cargo release.

GpG-containing PEMs restrain dendritic cell activation and TLR9 signalling *in vitro*

An important question is whether the assembly into and release from degradable PEMs impacts the immunomodulatory function of GpG. To answer this question, primary DCs were isolated and activated by the addition of CpG, a TLR9 agonist that stimulates inflammatory TLR9 signalling. The potential for GpG released from degradable PEMs to restrain this CpG-induced activation was then assessed. To ensure that sufficient mass of GpG would be released to test for effects in cell assays and to determine how long sequential assembly could be carried out, 100 bilayer-coated substrates were tested. These $(Poly1/GpG)_{100}$ coated substrates were incubated in buffer for defined time intervals of 1, 3, 5, or 7 days. Importantly, this process was also conducted using substrates coated with Poly1 and a control oligonucleotide (CTRL). CTRL has a similar structure to GpG but does not modulate TLR9 signalling. These compositions served as controls to isolate GpG-specific cargo effects. Flow cytometry analysis revealed incubation with soluble CpG drove high expression of activation markers CD80 (Fig. 4A), CD86 (Fig. 4B), and CD40 (Fig. 4C) relative to media only controls without toxicity (Fig. S1). This increased activation was

reflected by an increase in the percentage of live cells expressing high fluorescence signal when stained with antibodies against the indicated markers. Further, the addition of soluble GpG (positive control, light blue), but not soluble CTRL (negative control, light green), restrained the expression of these activation markers relative to CpG-treated controls. Treatment with release solutions from $(Poly1/GpG)_{100}$ down-regulated activation at all time points (Fig. 4A-4C, dark blue), indicating released GpG maintains function after incorporation into degradable PEMs and following release for up to seven days at 37°C. We also observed a trend of decreased activation as a function of the time of incubation for release. This result is likely driven by the corresponding increase in GpG dose with longer release times, consistent with kinetic studies (Fig. 3). Further, in some cases, the Poly1/GpG release solution exhibited more potent restraint of CpG-induced activation compared with the corresponding matched soluble dose. This observation could indicate that incorporation into and release from degradable PEMs alters and perhaps enhances the potency of free GpG. In contrast, minimal effects were observed from solutions released from $(Poly1/CTRL)_{100}$ coated substrates, with a small, but significant decrease in the expression of CD86 at day 7 and CD40 at days 5 and 7.

To explore the function of these cells, supernatants from cultures were analysed for the secretion of an early inflammatory cytokine, IL-6. Consistent with the activation data, supernatants of DCs incubated with CpG exhibited a dramatic upregulation of IL-6 secretion compared with media only controls (Fig. 4D). The addition of soluble GpG to CpG-treated wells (Fig. 4D, light blue bars) significantly restrained the level of IL-6 present in culture supernatants. The addition of soluble CTRL (Fig. 4D, light green bars) drove significant – though less potent than corresponding doses of GpG – restraint of IL-6 secretion, despite minimal effects on the expression of activation markers (Fig. 4A-C). Importantly, however, incubation of release solutions from Poly1/GpG PEMs (Fig. 4D, dark blue bars) were much more potent than levels caused by the background effect of CTRL. In fact, Poly1/GpG PEMs suppressed IL-6 secretion to levels similar to those observed with soluble GpG treatment. Addition of release solution from control PEMs again drove significant, though less potent relative to corresponding GpG-containing solutions, restraint of IL-6 levels (Fig. 4D, dark green bars). Together, these results suggest that assembly and release from degradable PEMs does not impair the potential for GpG to restrain inflammatory DC function.

To verify that GpG maintains molecular specificity following release, similar experiments were performed in which degradable PEM release solutions were collected and used to treat a TLR9 reporter cell line. As expected, a TLR9 agonist (CpG), but not a TLR4 agonist (lipopolysaccharide, LPS), upregulated TLR9 signalling, reflected in an increase in the secreted reporter (Fig. 5A). The addition of soluble GpG or GpG released from degradable PEMs to CpG-treated wells restrained signalling, resulting in significantly lower levels of TLR9 activity compared with CpG-treated control wells (Fig. 5A, dark blue and light blue bars). In contrast, wells treated with CpG and CTRL in either soluble form or from PEM release solutions exhibited high levels of signalling, with no significant differences in TLR9 activity relative to CpG-treated controls (Fig. 5A, dark green and light green bars). These results, consistent with findings in the primary DC studies, indicate that the potential for GpG to bind to its target receptor, TLR9, and modulate signalling activity is not compromised by incorporation into or release from PEMs.

GpG released from PEM assemblies limits inflammatory function, but not proliferation of transgenic T cells

To test the potential for Poly1/GpG PEMs to skew antigen-specific T cell function, we employed an *in vitro* model in which DCs from wild type C57BL/6J mice are co-cultured with MOG-reactive $CD4^+$ T cells isolated from transgenic 2D2 mice. Incubation of these T cells with a fluorescent dye (CFSE) prior to co-culture enables tracking of proliferation, as the dye is diluted through successive rounds of cell division. Flow cytometry analysis of co-cultures incubated with soluble MOG peptide and CpG revealed high levels of viability (Fig. 6A) and proliferation, indicated by a low median fluorescence intensity of CFSE signal (i.e., diluted dye) (Fig. 6B-C). In contrast, cultures that were not treated with MOG – media and CpG only controls – maintained high CFSE fluorescence signal. This result indicated that in the absence of antigen (MOG), the transgenic T cells were not triggered to proliferate. High levels of proliferation were observed when soluble CTRL was added to wells treated with MOG + CpG (Fig. 6C, light green bars). This effect was also observed when CTRL released from control degradable PEMs was added to cultures (Fig. 6C, dark green bars). Interestingly, despite significant effects on DC function and phenotype, no effect was observed on T cell proliferation when soluble GpG was added to cultures (Fig. 6C, light blue bars). Likewise, addition of Poly1/GpG release solutions caused relatively small effects on MOG + CpG-induced proliferation, with a modest, though significant, increase in CFSE signal intensity – corresponding to reduced proliferation – observed at day 7 (Fig. 6C, dark blue bars).

However, despite similar levels of proliferation, analysis of supernatants of these cultures revealed striking differences in cellular function. The positive control of MOG + CpG drove significant levels of IL-6 secretion in co-culture supernatants (Fig. 6D). The addition of soluble CTRL had no significant impact on the level of IL-6 (Fig. 6D, light green bars), while the addition Poly1/CTRL release solutions drove either no impact or small, but significant, decreases (Fig. 6D, dark green bars). In contrast, the addition of soluble GpG drove a large reduction in IL-6 secretion, with increased suppressive function observed at higher doses (Fig. 6D, light blue bars). Of note, the addition of Poly1/GpG release solution potently decreased the levels of IL-6, again exhibiting stronger effects at higher doses (i.e., longer release time) (Fig. 6D, dark blue bars) compared to the MOG + CpG control. Together, the results suggest that GpG released from degradable Poly1/GpG assemblies has minimal impact on the level of proliferation, but dramatically shifts the

function of expanding antigen-specific T cells away from pro-inflammatory activity.

GpG-containing PEM release solutions skew T cell phenotype towards regulatory populations

After observing restricted secretion of a pro-inflammatory cytokine, we hypothesized that degradable PEMs might also skew the phenotype of the proliferating antigen-specific T cells. To test this hypothesis, similar co-cultures of wild-type DCs and 2D2 T cells were set up and analysed by flow cytometry for the expression of key markers of regulatory T cells (T_{REGS}). In control cultures, we observed that the addition of CpG or MOG + CpG resulted in relatively low levels of T_{REGS}, defined as $CD4^+/CD25^+Foxp3^+$ cells (Fig. 7A), compared with cultures that received media only or MOG peptide only (Fig. 7B). The addition of soluble CTRL or Poly1/CTRL release solutions to wells treated with MOG + CpG exhibited low frequencies of T_{REGS}, similar to those observed in MOG + CpG controls. However, the addition of a soluble GpG (Fig. 7B, light blue bars) drove an increase in T_{REG} frequency at the highest dose, with a significant upregulation observed relative to the MOG + CpG control. Further, incubation with Poly1/GpG release solutions, resulted in a significant upregulation in T_{REG} proportion in both day 5 and day 7 samples (Fig. 7A-B, dark blue bars). Together, these results suggest that GpG skews T cell phenotype towards a tolerogenic population and that incorporation into degradable PEMs does not inhibit, and perhaps enhances, this potential.

Discussion

TLR9, along with other innate inflammatory pathways, has emerged as a potential target to restrain excess inflammation associated with autoimmune diseases. Recent strategies by our lab[16, 17] and others[26] have explored the use of biomaterials to control or enhance the delivery of regulatory TLR ligands. For example, Yu *et al.* conjugated a suppressive TLR9 oligonucleotide to a lipid designed to bind albumin, a platform that has been demonstrated to enhance delivery to key immune tissues, like lymph nodes.[26] Compared with free GpG, the lipid-conjugated oligonucleotide exhibited enhanced uptake and suppression of TLR9 signaling *in vitro* as well as restraint of adaptive immune responses *in vivo*. These results highlight the potential of biomaterials to tune and enhance the delivery of regulatory immune signals. Importantly, however, animal models of autoimmune diseases often develop over the course of weeks to months, and human diseases can span for decades. Further, previous studies have demonstrated elevated TLR signaling at different stages of disease in mice.[8] These findings support an interest to promote sustained delivery of anti-inflammatory therapeutics, as well as an opportunity to study the link between the kinetics of TLR antagonist delivery and the extent of tolerance during disease.

PEMs are well-suited to provide control over the delivery of GpG, as the inherent charged nature of the components of interest – a cationic polymer and an oligonucleotide – enable electrostatically-driven self-assembly. Further, the potential to tune absolute and relative cargo levels in layer-by-layer coatings over a range of length scales has supported the application of PEMs to a wide range of fields, including drug delivery, and, more recently, immunotherapy.[20, 27-30] Yet, PEMs remain largely unexplored in the context of autoimmune disease and towards the goal of promoting immune tolerance. Our results demonstrate the potential to employ PEM technology to release functional GpG over time, and future experiments could further exploit the modular nature of PEMs to explore open questions. For example, alternative polymers with varying molecular weight and other properties could be incorporated into formulations to expand or tune release kinetics.

Further, more detailed analyses of the release solutions could provide insight into the nature of GpG released from degradable PEMs. In some cases, we observed the efficacy of GpG from degradable PEM release solution was higher than that of free GpG, such as in a significant polarization towards T_{REGS} at a lower dose relative to that of soluble GpG (Fig. 7B). To investigate the cause of this enhanced function, the association state of GpG in release solutions could be tested to determine whether released GpG is in a different physical form (e.g., complexed with Poly1) after release from PEMs. These associations might facilitate cellular uptake or alter cellular trafficking by enhancing interaction with TLR9 receptors localized in endosomes, resulting in more potent suppression of inflammation.[31, 32] These studies could also serve to explore the background suppressive effects we observed in soluble CTRL or Poly1/CTRL release solution samples in the TLR9 signaling assays (Figure 5). This area of exploration could be of particular relevance, because physiochemical characteristics of polymers and other biomaterials, such as charge, size, molecular weight, and hydrophobicity, have been shown to impact inflammatory signaling, even in the absence of other immune cues[23, 33-35]. Thus, together these studies could elucidate properties of released vs. free GpG and CTRL that might drive differences observed in inflammatory cell phenotype and function. In parallel, profiling the function of GpG-containing degradable PEMs *in vivo* would determine the potential to regulate inflammation during active disease. These experiments could compare coating and delivery of a macro- or micro-scale substrate (e.g., implantable device, particles on the order of 50-100 μm) with administration of coated nano- or microparticles that could be internalized by DCs and other antigen presenting cells. This exploration could examine and compare the effects of slow, controlled release in the extracellular space with an approach that could enhance localization of GpG cargo with TLR9 in endosomes, as described above, respectively. These studies could also incorporate characterization of key cell phenotypes (e.g., T_H1, T_H17) that typically cause disease and the potential to limit associated cytokine secretion (e.g., IL-17) and bias cells towards regulatory populations. These cell populations of interest in animal models, such as EAE, have also been identified as key contributors in human MS and other diseases;

thus, these studies could provide insight into potential for clinical translation.

Finally, our current results demonstrate the potential to skew antigen-specific T cell function during proliferation away from inflammation and towards T_{REGS} (Figures 6-7). Yet, the myelin-specific signal is not incorporated into the PEM itself, as our current results sought to explore the role of kinetic release. One area of interest could be to incorporate myelin peptide, along with Poly1, as a component of PEMs to enable both programmable release and antigen specificity. This application could be of interest as the potential to induce tolerance through co-delivery of antigen and regulatory signal has been highlighted by recent work.[16, 36-39] This question could be addressed by alternating cationic layers of Poly1 and modified MOG peptide,[16] or by blending Poly1 and MOG in defined ratios to form the cationic cargo solution. The modular nature of the PEM platform would also allow for facile substitution with alternative self-antigens of interest for type 1 diabetes, systemic lupus erythematosus, or other autoimmune disorders.

Conclusions

Our results reveal an approach to control the release of an antagonist to inflammatory signalling over time without loss of biologic function, suggesting an opportunity to control chronic inflammation associated with autoimmunity. There are a number of open questions of interest, such as the potential to regulate TLR9 signalling and control clinical symptoms of disease and underlying inflammation *in vivo*. There is also potential to exploit the modular nature of this approach to introduce antigen or other signals of interest to enhance the specificity and selectivity of tolerance, critical criteria for the development of new clinical therapies.

Conflicts of interest

C.M.J. is an employee of the VA Maryland Health Care System. The views reported in this paper do not reflect the views of the Department of Veterans Affairs or the United States Government. C.M.J. has an equity position in Cellth Systems, LLC.

Acknowledgements

L.H.T. is a National Science Foundation Graduate Fellow (# DGE1322106). H.B.E. is a trainee of the NIH T32 Training Program in Cell and Molecular Biology (T32GM080201). B.X. is a Maryland-Howard Hughes Medical Institute Undergraduate Research Fellow. This work was supported in part by the United States Department of Veterans Affairs (Award # 1I01BX003690), the National Institutes of Health (Award # R01EB026896), NSF CAREER Award # 1351688, and a grant to the University of Maryland from the Howard Hughes Medical Institute through the Science Education Program.

Notes and references

1 L. L. Aung, P. Fitzgerald-Bocarsly, S. Dhib-Jalbut and K. Balashov, *J Neuroimmunol*, 2010, **226**, 158-164.
2 K. E. Balashov, L. L. Aung, A. Vaknin-Dembinsky, S. Dhib-Jalbut and H. L. Weiner, *Ann Neurol*, 2010, **68**, 899-906.
3 T. Celhar, R. Magalhaes and A. M. Fairhurst, *Immunol Res*, 2012, **53**, 58-77.
4 K. Derkow, J. M. Bauer, M. Hecker, B. K. Paap, M. Thamilarasan, D. Koczan, E. Schott, K. Deuschle, J. Bellmann-Strobl, F. Paul, U. K. Zettl, K. Ruprecht and S. Lehnardt, *PLoS One*, 2013, **8**, e70626.
5 P. N. Kelly, D. L. Romero, Y. Yang, A. L. Shaffer, 3rd, D. Chaudhary, S. Robinson, W. Miao, L. Rui, W. F. Westlin, R. Kapeller and L. M. Staudt, *J Exp Med*, 2015, **212**, 2189-2201.
6 J. M. Reynolds, G. J. Martinez, Y. Chung and C. Dong, *Proc Natl Acad Sci U S A*, 2012, **109**, 13064-13069.
7 M. Santoni, K. Andrikou, V. Sotte, A. Bittoni, A. Lanese, C. Pellei, F. Piva, A. Conti, M. Nabissi, G. Santoni and S. Cascinu, *Cancer Treat Rev*, 2015, **41**, 569-576.
8 M. Prinz, F. Garbe, H. Schmidt, A. Mildner, I. Gutcher, K. Wolter, M. Piesche, R. Schroers, E. Weiss, C. J. Kirschning, C. D. Rochford, W. Bruck and B. Becher, *J Clin Invest*, 2006, **116**, 456-464.
9 P. P. Ho, P. Fontoura, P. J. Ruiz, L. Steinman and H. Garren, *J Immunol*, 2003, **171**, 4920-4926.
10 P. P. Ho, P. Fontoura, M. Platten, R. A. Sobel, J. J. DeVoss, L. Y. Lee, B. A. Kidd, B. H. Tomooka, J. Capers, A. Agrawal, R. Gupta, J. Zernik, M. K. Yee, B. J. Lee, H. Garren, W. H. Robinson and L. Steinman, *J Immunol*, 2005, **175**, 6226-6234.
11 A. H. Cross and R. T. Naismith, *J Intern Med*, 2014, **275**, 350-363.
12 O. Khan, P. Rieckmann, A. Boyko, K. Selmaj and R. Zivadinov, *Annals of Neurology*, 2013, **73**, 705-713.
13 J. S. Wolinsky, T. E. Borresen, D. W. Dietrich, D. Wynn, Y. Sidi, J. R. Steinerman, V. Knappertz and S. Kolodny, *Multiple Sclerosis and Related Disorders*, 2015, **4**, 370-376.
14 M. L. Bookstaver, S. J. Tsai, J. S. Bromberg and C. M. Jewell, *Trends in Immunology*, 2018, **39**, 135-150.
15 L. H. Tostanoski and C. M. Jewell, *Advanced Drug Delivery Reviews*, 2017, **114**, 60-78.
16 L. H. Tostanoski, Y. C. Chiu, J. I. Andorko, M. Guo, X. Zeng, P. Zhang, W. Royal, 3rd and C. M. Jewell, *ACS Nano*, 2016, DOI: 10.1021/acsnano.6b04001.
17 K. L. Hess, J. I. Andorko, L. H. Tostanoski and C. M. Jewell, *Biomaterials*, 2017, **118**, 51-62.
18 G. Decher and J. D. Hong, *Makromol Chem-M Symp*, 1991, **46**, 321-327.
19 E. Donath, G. B. Sukhorukov, F. Caruso, S. A. Davis and H. Mohwald, *Angewandte Chemie-International Edition*, 1998, **37**, 2202-2205.
20 Y. Yan, M. Bjonmalm and F. Caruso, *Chem Mater*, 2014, **26**, 452-460.
21 D. M. Lynn and R. Langer, *Journal of the American Chemical Society*, 2000, **122**, 10761-10768.
22 R. B. Shmueli, D. G. Anderson and J. J. Green, *Expert opinion on drug delivery*, 2010, **7**, 535-550.
23 J. I. Andorko, K. L. Hess, K. G. Pineault and C. M. Jewell, *Acta Biomater*, 2016, **32**, 24-34.
24 Y. C. Chiu, J. M. Gammon, J. I. Andorko, L. H. Tostanoski and C. M. Jewell, *ACS Appl Mater Interfaces*, 2016, **8**, 18722-18731.
25 Q. Zeng, J. M. Gammon, L. H. Tostanoski, Y. C. Chiu and C. M. Jewell, *ACS Biomater Sci Eng*, 2017, **3**, 195-205.
26 C. Yu, M. An, E. Jones and H. Liu, *Pharm Res*, 2018, **35**, 56.
27 P. C. DeMuth, Y. Min, B. Huang, J. A. Kramer, A. D. Miller, D.

H. Barouch, P. T. Hammond and D. J. Irvine, *Nat Mater*, 2013, **12**, 367-376.
28 J. Cui, R. De Rose, J. P. Best, A. P. Johnston, S. Alcantara, K. Liang, G. K. Such, S. J. Kent and F. Caruso, *Adv Mater*, 2013, **25**, 3468-3472.
29 S. De Koker, K. Fierens, M. Dierendonck, R. De Rycke, B. N. Lambrecht, J. Grooten, J. P. Remon and B. G. De Geest, *J Control Release*, 2014, **195**, 99-109.
30 B. G. De Geest, M. A. Willart, B. N. Lambrecht, C. Pollard, C. Vervaet, J. P. Remon, J. Grooten and S. De Koker, *Angew Chem Int Ed Engl*, 2012, **51**, 3862-3866.
31 M. L. Bookstaver, K. L. Hess and C. M. Jewell, *Small*, 2018, **14**, 1802202.
32 S. J. Tsai, J. I. Andorko, X. Zeng, J. M. Gammon and C. M. Jewell, *Nano Research*, 2018, **11**, 5642-5656.
33 N. A. Hotaling, L. Tang, D. J. Irvine and J. E. Babensee, in *Annual Review of Biomedical Engineering, Vol 17*, ed. M. L. Yarmush, Annual Reviews, Palo Alto, 2015, vol. 17, pp. 317-349.
34 F. A. Sharp, D. Ruane, B. Claass, E. Creagh, J. Harris, P. Malyala, M. Singh, D. T. O'Hagan, V. Petrilli, J. Tschopp, L. A. O'Neill and E. C. Lavelle, *Proc Natl Acad Sci U S A*, 2009, **106**, 870-875.
35 D. F. Moyano, M. Goldsmith, D. J. Solfiell, D. Landesman-Milo, O. R. Miranda, D. Peer and V. M. Rotello, *J Am Chem Soc*, 2012, **134**, 3965-3967.
36 L. H. Tostanoski, Y. C. Chiu, J. M. Gammon, T. Simon, J. I. Andorko, J. S. Bromberg and C. M. Jewell, *Cell Rep*, 2016, **16**, 2940-2952.
37 R. A. Maldonado, R. A. LaMothe, J. D. Ferrari, A. H. Zhang, R. J. Rossi, P. N. Kolte, A. P. Griset, C. O'Neil, D. H. Altreuter, E. Browning, L. Johnston, O. C. Farokhzad, R. Langer, D. W. Scott, U. H. von Andrian and T. K. Kishimoto, *Proc Natl Acad Sci U S A*, 2015, **112**, E156-165.
38 L. Northrup, M. A. Christopher, B. P. Sullivan and C. Berkland, *Adv Drug Deliv Rev*, 2016, **98**, 86-98.
39 A. Yeste, M. Nadeau, E. J. Burns, H. L. Weiner and F. J. Quintana, *Proc Natl Acad Sci U S A*, 2012, **109**, 11270-11275.

Figure Captions

Fig. 1 Qualitative and quantitative analyses reveal layer-dependent incorporation of fluorescent GpG into degradable PEMs. (A) Fluorescence microscopy images and (B) pixel intensity plots of planar quartz substrates, coated with the indicated number of Poly1/Cy5-GpG bilayers, following removal of a portion of the film with a needle scratch (Panel A, scale bar: 50μm). In separate studies, polystyrene microparticles coated with 1, 2, or 3 Poly1/Cy5-GpG bilayers were analysed by (C) fixed exposure time fluorescence microscopy imaging and (D) pixel intensity quantification (Panel C, scale bar: 5μm).

Fig. 2 Degradable PEMs exhibit a linear increase in thickness and cargo loading with increasing numbers of bilayers. Thickness of degradable Poly1/GpG PEMs, deposited onto base layer-coated silicon substrates, quantified by ellipsometry (A) every two bilayers through eight bilayers or (B) every eight bilayers through 56 Poly1/GpG bilayers. Data represent mean ± SEM (n = 4). Spectrophotometric analysis of relative GpG loading (260 nm) of quartz substrates through (C) eight or (D) 56 Poly1/GpG bilayers. Data indicate representative mean ± SEM (n = 3) of one of at least four similar experiments. (E) Average spectrophotometric scans of quartz substrates shown in (D) after deposition of the indicated number of Poly1/GpG bilayers.

Fig. 3 Poly1/GpG PEMs exhibit time-dependent degradation and cargo release. (A) Quantification of GpG release from silicon substrates coated with (Poly1/GpG)100 after incubation in 1X PBS at 37°C for the indicated time intervals. (B) Relative loading of GpG on quartz substrates coated with (Poly1/GpG)100, incubated for defined time intervals as in (A). The corresponding release of GpG into solution from incubation of substrates in Panel (B) was quantified by spectrophotometry. In Panels (A) and (C), spectrophotometric absorbance (260nm) was converted to GpG mass using a known standard. Data in all panels represent mean SEM ± (n=3).

Fig. 4 GpG-containing degradable PEMs down-regulate DC activation and secretion of inflammatory cytokines. Splenic DCs were incubated with media, soluble CpG, or soluble CpG with the addition of GpG or CTRL, either in release solutions from PEM-coated substrates incubated for indicated intervals, or as dose-matched soluble controls. The GpG or CTRL doses for days 1, 3, 5, and 7, were 1.30 μg, 4.13 μg, 8.20 μg, and 11.30 μg, respectively. Expression of (A) CD80, (B) CD86, and (C) CD40, following 16 h of incubation, was quantified by flow cytometry. (D) Supernatants from cultures in (A-C) were analysed for the secretion of IL-6. Values in all panels indicate mean ± SEM of studies conducted in triplicate. Data were analysed with one-way ANOVA with a Tukey post-test. For clarity, only key comparisons are shown, comparing all samples to the CpG Only control. (* = P ≤ 0.05; ** = P ≤ 0.01; *** = P ≤ 0.001; **** = P ≤ 0.0001).

Fig. 5 Poly1/GpG PEMs downregulate TLR9 signalling in vitro. Quantification of TLR9 activity in reporter cells following 18 h incubation with TLR9 agonist CpG alone, or CpG in addition to release solutions from (Poly1/GpG)100 or (Poly1/CTRL)100 coated substrates or matched soluble doses. The GpG or CTRL doses for days 1, 3, 5, and 7, were 2.32 μg, 2.93 μg, 3.85 μg, and 7.55 μg, respectively. A control of a TLR4 agonist, LPS, was included to verify pathway specificity. Values in all panels indicate mean ± SEM of studies conducted in triplicate. Data were analysed with one-way ANOVA with a Tukey post-test. For clarity, only key comparisons are shown, comparing all samples to the CpG control. (** = P ≤ 0.01; **** = P ≤ 0.0001).

Fig. 6 GpG-containing PEMs skew proliferating antigen-specific T cell function away from inflammation. Co-cultures of wild-type DCs and transgenic MOG-reactive T cells were prepared. Cultures were incubated with combinations of MOG, CpG, GpG, and CTRL for control wells (gray bars). Experimental wells were activated with soluble MOG and soluble GpG, and then release solutions from (Poly1/GpG)100 or (Poly1/CTRL)100 coated substrates or matched soluble doses were added. The GpG or CTRL doses for days 1, 3, 5, and 7, were 1.30 μg, 4.13 μg, 8.20 μg, and 11.30 μg, respectively. After 72 h of co-culture (A) viability (i.e., DAPI-) and (B-C) proliferation of T cells was analysed by flow cytometry. To quantify proliferation, T cells were labelled with a fluorescent dye (CFSE) before culture; as cells undergo successive rounds of proliferation, CFSE is diluted among dividing cells, resulting in a reduced median fluorescence intensity (MFI) of signal. B) Representative histograms and C) average MFI of CFSE signal are shown. C) Supernatants from cultures in (A-B) were analysed for secretion of inflammatory IL-6. Values in all panels indicate mean ± SEM of studies conducted in triplicate. Data were analysed with one-way ANOVA with a Tukey post-test. For clarity, only key comparisons are shown, comparing all samples to the MOG + CpG control. (* = P ≤ 0.05; ** = P ≤ 0.01; *** = P ≤ 0.001; **** = P ≤ 0.0001).

Fig. 7 Degradable Poly1/GpG PEMs polarize antigen-specific T cells towards TREGS. Wild-type DCs were co-cultured with transgenic MOG-specific T cells. Co-cultures were incubated with media, MOG only, CpG only, or MOG + CpG as controls (gray bars). Experimental wells were activated with soluble MOG and soluble CpG, and then release solutions from (Poly1/GpG)100 or (Poly1/CTRL)100 coated substrates or matched soluble doses were added. The GpG or CTRL doses for days 1, 3, 5, and 7, were 1.33 μg, 4.49 μg, 6.20 μg, and 7.91 μg, respectively. After 72 h of co-culture, the expression of CD25 and Foxp3 among CD4+ cells was assessed by flow cytometry. (A) Representative scatter plots of CD25 and Foxp3 expression among CD4+ cells. (B) Mean frequency of CD4+/CD25+Foxp3+ in co-cultures, using the gating scheme shown in (A). Values in Panel B indicate mean ± SEM of studies conducted in triplicate. Data were analysed with one-way ANOVA with a Tukey post-test. For clarity, only key comparisons are shown, comparing all samples to the MOG + CpG control. (** = P ≤ 0.01; **** = P ≤ 0.0001).

TOC Entry Degradable polyelectrolyle multilayers to enable controlled release of a regulatory toll-like receptor ligand to restrain inflammation and promote immune tolerance.

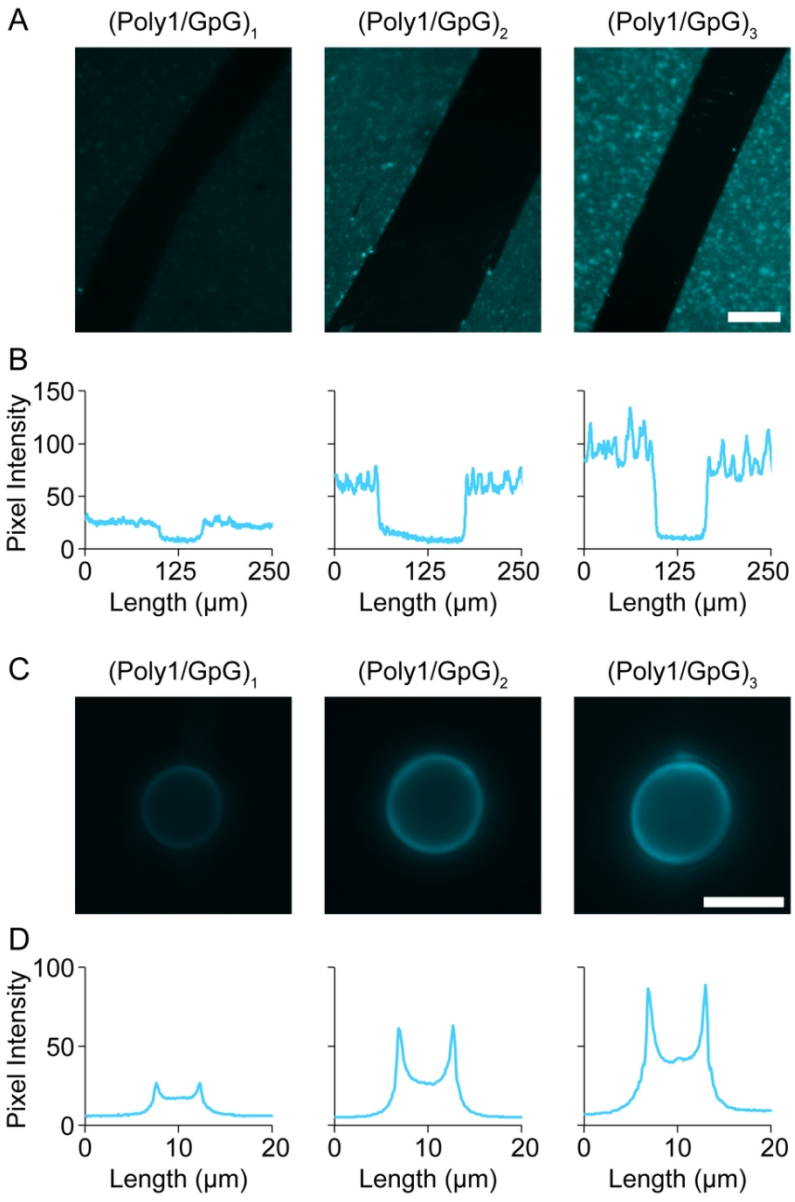

Figure 1

82x123mm (300 x 300 DPI)

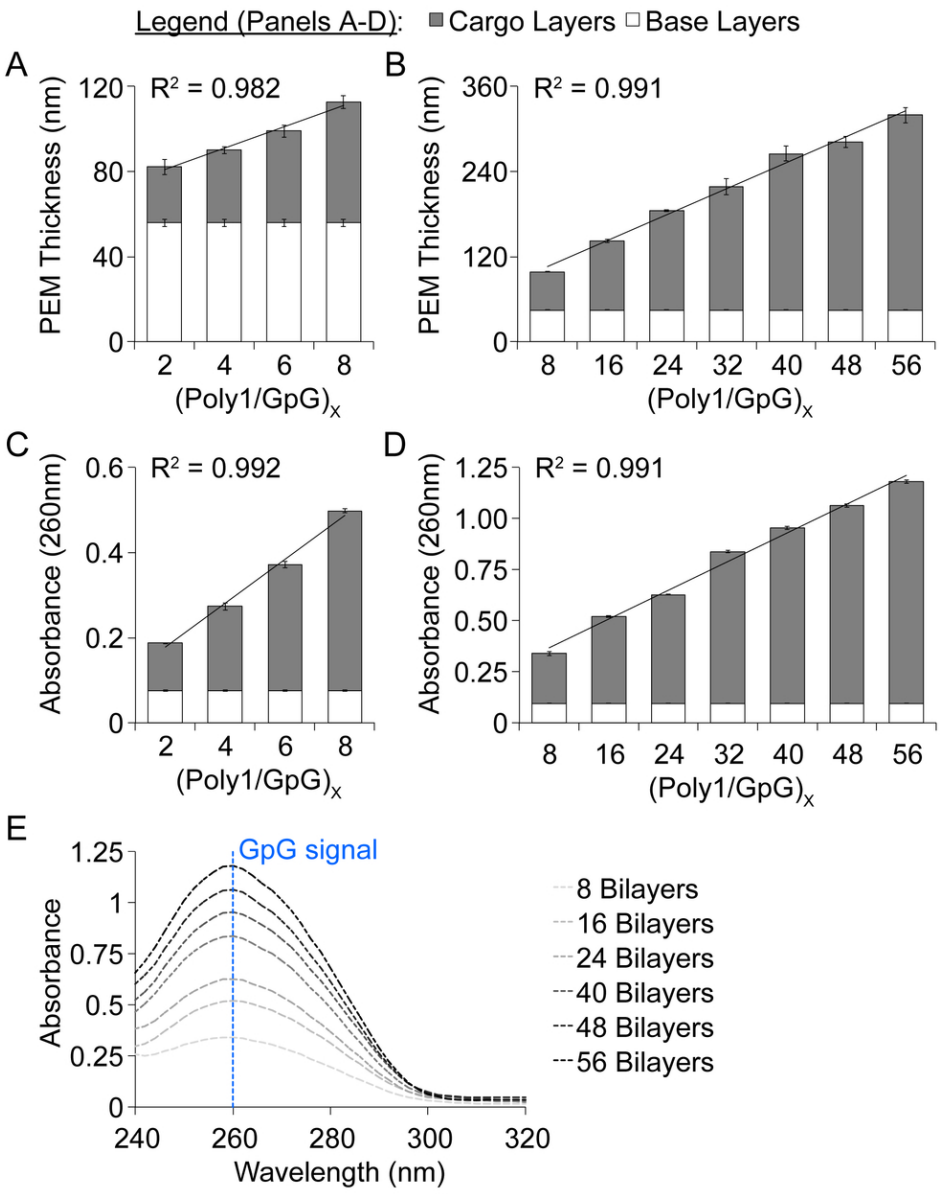

Figure 2

82x106mm (300 x 300 DPI)

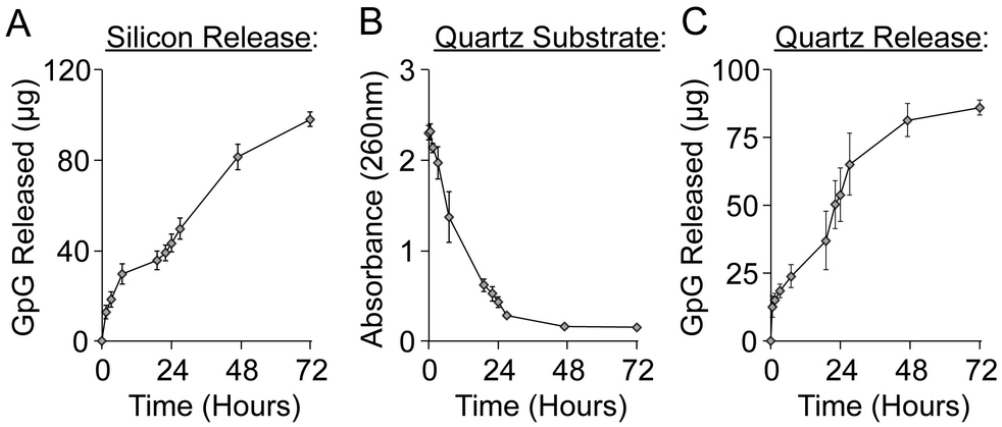

Figure 3

82x35mm (300 x 300 DPI)

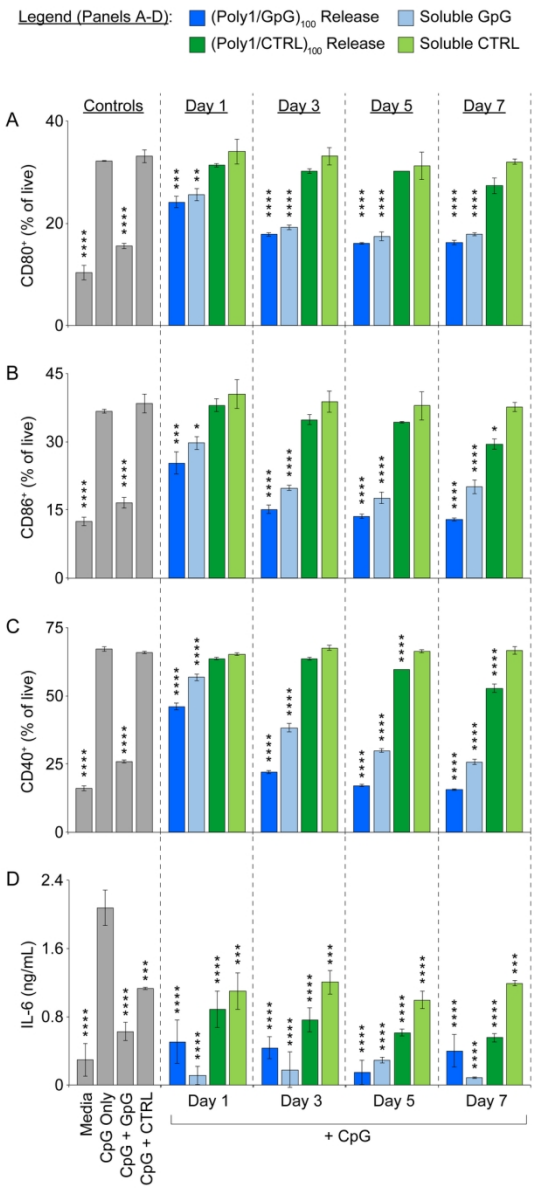

Figure 4

82x183mm (300 x 300 DPI)

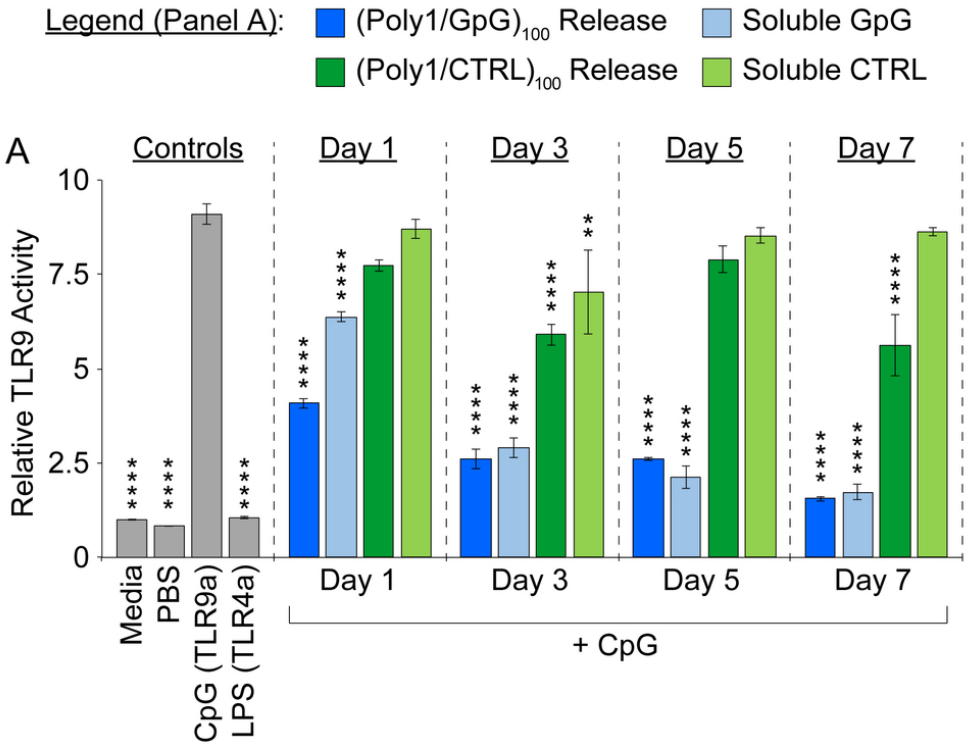

Figure 5

82x63mm (300 x 300 DPI)

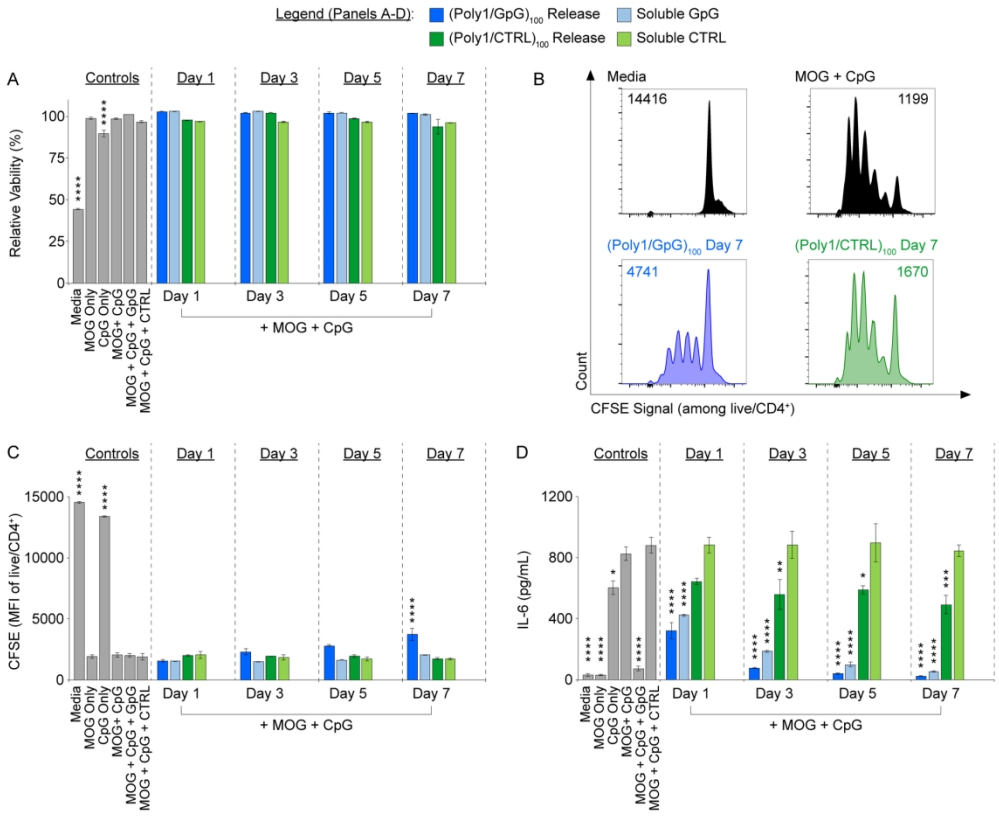

Figure 6

171x140mm (300 x 300 DPI)

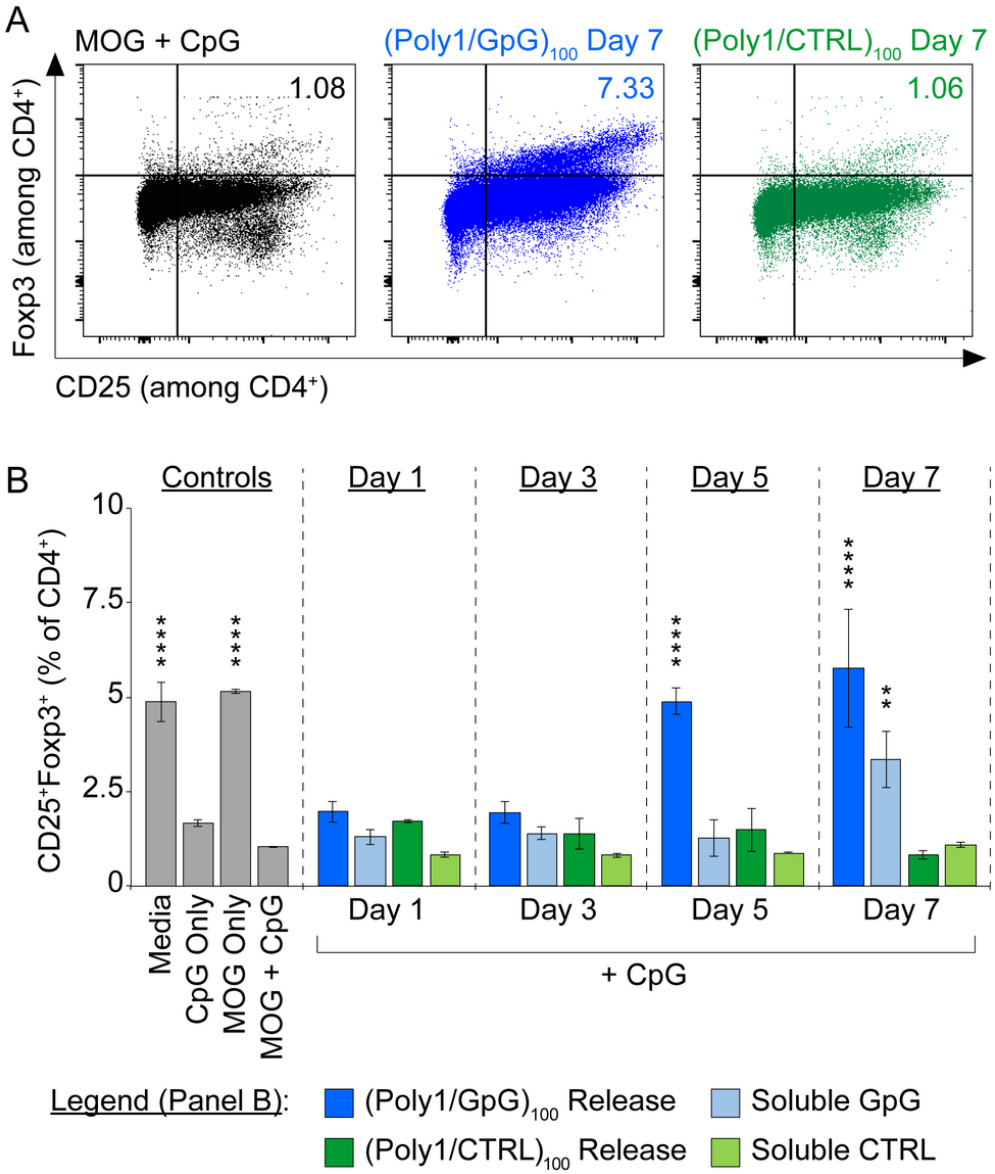

Figure 7

82x98mm (300 x 300 DPI)

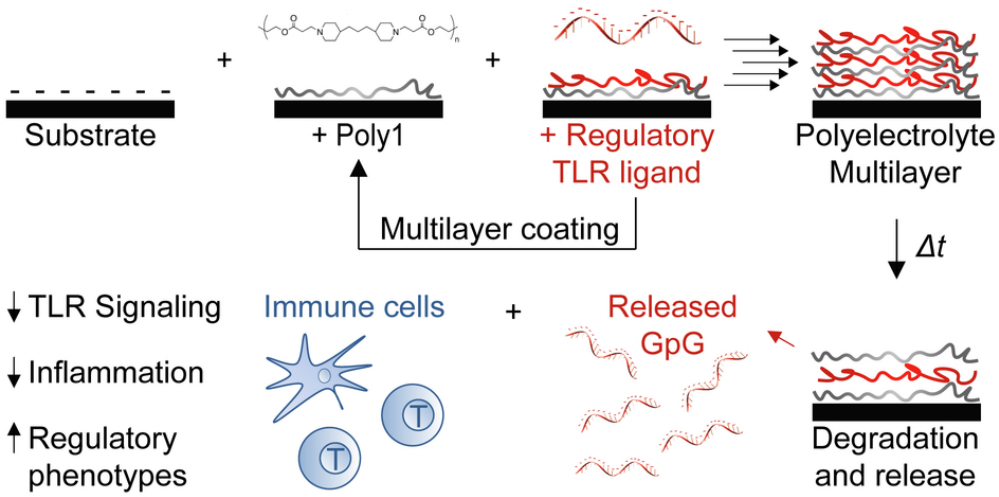

80x40mm (300 x 300 DPI)